REVISTA INTERDISCIPLINAR DE PESQUISA EM ENGENHARIA

CILAMCE 2016
XXXVII IBERIAN LATIN AMERICAN CONGRESS ON COMPUTATIONAL METHODS IN ENGINEERING
BRASÍLIA - DF - BRAZIL

3D FINITE ELEMENT MODEL FOR THERMO-PORO-MECHANICAL DEFORMATION IN SEDIMENTARY BASINS

André R. Brüch

Paulo S. B. Lemos

Samir Maghous

andrebruch@hotmail.com

paulobaumbach@hotmail.com

samir.maghous@ufrgs.br

Federal University of Rio Grande do Sul, Department of Civil Engineering

Av. Osvaldo Aranha 99, 3rd floor, Centro – CEP 90035-190 – Porto Alegre, RS, Brazil

Abstract. *Sedimentary basins form when an appreciable amount of sediments are deposited along geological time and transformed into rock through natural phenomena known as diagenesis. Compaction of sediments, fluid and thermal flows are fundamental coupled processes in sedimentary basin modelling. Purely mechanical phenomena prevail in the upper layers involving pore fluid expulsion and rearrangement of solid particles, while chemo-mechanical compaction resulting from Intergranular Pressure-Solution (IPS) dominates for deeper burial as stress and temperature increase. The thermal evolution of the basin may substantially affect both processes as heat modifies fluid viscosity and physicochemical properties of minerals, thus affecting fluid flow and mineral stability. The aim of the present contribution is to provide a comprehensive 3D framework for constitutive and numerical modelling of thermo-poro-mechanical deformation during diagenesis. Purely mechanical and chemo-mechanical deformations are respectively modelled by means of poroplastic and poroviscoplastic models. The numerical simulations are performed through the finite element method with a shared memory multiprocessing interface. The sedimentary basin is modelled as a fully saturated thermo-poro-elasto-visco-plastic material undergoing large strains. Special attention is given to temperature effects on the deformation history of the basin.*

Keywords: *Sedimentary basin, Thermo-poro-mechanics, Thermo-poro-elasto-visco-plasticity.*

1 INTRODUCTION

The study of sedimentary basins is an important subject in the field of geophysics and geomechanics that seeks understanding the geological history of the planet. It is also of great economic importance as the formation of natural hydrocarbons such as oil, gas and coal takes place almost entirely within sedimentary rocks. In connection with many petroleum engineering activities, predicting the porosity reduction history in sedimentary basins is a fundamental issue as porosity profile strongly affects oil migration, trapping and excess pore-pressure build-up. However, accurate assessment of porosity distribution still remains a complex task that requires a comprehensive modelling of the sediment behavior in the context of large strains and multiple coupled processes. In this respect, basin modelling seeks to reconstruct the thermo-poro-mechanical state of sedimentary basins by simulating different geological events that occurred throughout its formation and deformation history.

From the mechanical point of view, two deformation mechanisms control the compaction process of sediments. Purely mechanical phenomena prevails in the upper layers of the basin involving pore fluid expulsion and rearrangement of solid particles, while chemo-mechanical compaction resulting from Intergranular Pressure-Solution *(IPS)* dominates for deeper burial as stress and temperature increase (Schmidt and McDonald, 1979). However, there is a transition zone where mechanical and chemo-mechanical compactions occur as strongly interdependent processes. The location of the transition zone ranges from a depth of a few hundred meters to more than a kilometer depending on the nature of the porous material and field conditions (Schneider et al., 1996).

The thermal evolution of the basin may substantially affect both compaction processes as heat modifies fluid viscosity and physicochemical properties of minerals, thus affecting fluid flow and mineral stability. Temperature increases with depth and depends on factors such as mantle heat flow, radioactive processes and thermal conductivity of the porous material, which evolves with porosity as the thermal conductivity of fluids and minerals may be quite different (Bjorlykke, 2010). The combined effects of deformation and heat flow control the rate and extent of hydrocarbon maturation in potential source rocks, which is of prime interest in oilfield appraisal (Palumbo et al., 1999).

The aim of the present contribution is to provide a comprehensive 3D framework for constitutive and numerical modelling of thermo-poro-mechanical deformation processes during diagenesis. Purely mechanical and chemo-mechanical deformations are respectively modelled by means of poroplastic and poroviscoplastic models. A key feature of the model is related to the evolution of the sediment material properties associated with temperature and large irreversible porosity changes. The numerical simulations are performed through the finite element method with a shared memory multiprocessing interface. The implementation allows for numerical simulation of sediments accretion/erosion periods by progressive activation/deactivation of the gravity forces within a fictitious closed material system.

The sedimentary basin is modelled as a fully saturated thermo-poro-elasto-visco-plastic material undergoing large strains. An oceanic basin is represented on a simplified geological setting as a horizontal infinite layer where sediments deposition occurs over tens of millions of years. As the gravitational compaction proceeds, several aspects of diagenesis are reproduced within the model. The basin mesh is made up by a single column of elements under oedometric conditions. The evolution in time of the porous material constitutive model is presented and analyzed in conjunction with the overall behavior of the sedimentary basin. Special attention is given to temperature effects on the deformation history of the basin.

2 THERMO-PORO-MECHANICAL CONSTITUTIVE MODEL

At the macroscopic scale, a porous medium can be viewed as the superposition of a solid continuum related to the deformable skeleton and a fluid phase occupying the porous space. In order to define the thermo-poro-mechanical problem under quasi-static conditions, three governing equations referring to momentum, mass and entropy balance must be specified. Disregarding the inertial effects, the equilibrium equation for the porous continuum is:

$$\operatorname{div}\underline{\underline{\sigma}} + \rho \underline{g} = 0 \tag{1}$$

where $\underline{\underline{\sigma}}$ is the Cauchy total stress tensor, $\underline{g}$ is the acceleration of gravity and $\rho = \varphi\rho^f + (1-\varphi)\rho^s$ is the density of the porous material, which can be computed from the Eulerian porosity φ (i.e. the pore volume fraction in the current configuration), the fluid density ρ^f and the solid grains density ρ^s.

Denoting by $\phi = J\varphi$ the Lagrangian porosity, where J is the Jacobian of the geometrical transformation of the skeleton particle, the equation referring to the fluid mass balance is:

$$\frac{d}{dt}\left(\rho^f \phi\right) + J \operatorname{div}\left(\rho^f \underline{q}^f\right) = 0 \tag{2}$$

where $\underline{q}^f$ is the filtration vector defined according to Darcy's law:

$$\underline{q}^f = \underline{\underline{K}}^f \cdot \left(-\underline{\nabla} p + \rho^f \underline{g}\right) \tag{3}$$

where p is the pore-pressure and $\underline{\underline{K}}^f$ is the permeability tensor, which is reduced to $\underline{\underline{K}}^f = k^f \underline{\underline{1}}$ when isotropy is taken into account.

The thermo-poro-mechanical approach at the macroscopic scale considers that the solid and fluid phases of the porous elementary volume are in thermal equilibrium at any instant of time. Considering that conduction is the dominant mode of heat transfer in the basin and disregarding the effects of mechanical dissipation associated with the fluid and solid skeleton, the entropy balance equation is:

$$\rho c \frac{dT}{dt} + \operatorname{div}\underline{q}^t = r^t \tag{4}$$

where c is the specific heat capacity at constant pressure and volume, T is the temperature, r^t is the heat generation per unit volume, usually associated to radioactive processes, and $\underline{q}^t$ is the heat flow vector, defined by Fourier's law:

$$\underline{q}^t = -\underline{\underline{K}}^t \cdot \underline{\nabla} T \tag{5}$$

where $\underline{\underline{K}}^t$ is the thermal conductivity tensor, which in case of isotropy becomes $\underline{\underline{K}}^t = k^t \underline{\underline{1}}$.

In the framework of large irreversible strains, the constitutive behavior of the sediment material is defined by two state equations, together with complementary relations associated to the flow rule structure. It is assumed that the elastic part of the deformation gradient of the skeleton particles remains infinitesimal, which implies that large strains involved during compaction process are essentially irreversible. In addition, the sediment material is assumed to exhibit isotropic properties disregarding anisotropy induced by compaction process. In this context, the macroscopic rate equations of state have been formulated within the framework of finite thermo-poro-elasto-visco-plasticity by extending the isothermal model presented in Brüch et al. (2016) to deal with temperature effects on the constitutive behavior of the porous material. The first state equation relates the stress rate $\dot{\underline{\underline{\sigma}}}$, pore pressure rate $\dot{p}$ and temperature rate $\dot{T}$ to the strain rate tensor $\underline{\underline{d}}$:

$$\frac{D_J \underline{\underline{\sigma}}'^{te}}{Dt} = \dot{\underline{\underline{\sigma}}}'^{te} + \underline{\underline{\sigma}}'^{te} \cdot \underline{\underline{\Omega}} - \underline{\underline{\Omega}} \cdot \underline{\underline{\sigma}}'^{te} = \dot{\underset{\sim}{C}} : \underset{\sim}{C}^{-1} : \underline{\underline{\sigma}}'^{te} + \underset{\sim}{C} : \left(\underline{\underline{d}} - \underline{\underline{d}}^{ir} \right) \tag{6}$$

where $\underline{\underline{d}}^{ir} = \underline{\underline{d}}^{p} + \underline{\underline{d}}^{vp}$ stands for the irreversible strain rate, $\underline{\underline{d}}^{p}$ (resp. $\underline{\underline{d}}^{vp}$) is the plastic (resp. viscoplastic) strain rate, while $\underline{\underline{\Omega}}$ is the rotation (spin) rate tensor which aims at taking the large rotation of the elementary volume into account. The fourth-order tensor $\underset{\sim}{C}$ contains the material drained elastic moduli and expresses by virtue of isotropy assumption:

$$\underset{\sim}{C} = \left(K - 2\mu/3 \right) \underline{\underline{1}} \otimes \underline{\underline{1}} + 2\mu \underset{\sim}{1} \tag{7}$$

where K and μ are the bulk and shear modulus, respectively. $\underline{\underline{1}}$ and $\underset{\sim}{1}$ denote respectively the second and fourth-order identity tensors. Equation (6) involves a rotational time derivative D_J/Dt of the effective stress tensor $\underline{\underline{\sigma}}'^{te} = \underline{\underline{\sigma}} + bp\underline{\underline{1}} + 3K\alpha^s \Delta T \underline{\underline{1}}$, which is a generalization of the Biot effective stress classically considered in isothermal conditions, where b denotes the Biot coefficient and α^s the thermal dilation coefficient of the solid phase (Coussy, 2004). It also includes a term related to the particulate derivative $\dot{\underset{\sim}{C}}$ of the tensor of drained elastic moduli $\underset{\sim}{C}$, which aims at capturing the evolution of the elastic properties with the microstructural changes due to large irreversible strains (Dormieux and Maghous, 2000).

The second state equation relates the pore volume change rate $\dot{\phi}$ to the rate $\dot{p}$ of the pore pressure, temperature rate $\dot{T}$ and to the strain rate $\underline{\underline{d}}$:

$$\dot{p} = M \left(\frac{\dot{\phi} - \dot{\phi}^{ir}}{J^{ir}} - \dot{b} \operatorname{tr}\left(\underset{\sim}{C}^{-1} : \underline{\underline{\sigma}}'^{te} \right) - b \operatorname{tr}\left(\underline{\underline{d}} - \underline{\underline{d}}^{ir} \right) + 3\dot{\alpha}^{\phi} \Delta T + 3\alpha^{\phi} \dot{T} \right) + \frac{\dot{M}}{M} p \tag{8}$$

where M is the Biot modulus, ϕ^{ir} is the irreversible part of the Lagrangian porosity variation, α^{ϕ} is the thermal dilation coefficient related to the porosity and $J^{ir} = J^{p} J^{vp}$ is the irreversible part of the Jacobian of transformation. J^{p} and J^{vp} are, respectively, the plastic and viscoplastic parts of the Jacobian of transformation. The terms involving $\dot{M}$, $\dot{b}$ and $\dot{\alpha}^{\phi}$ are related to the influence of large irreversible strains on the poroelastic properties.

The solid phase constituting the skeleton is assumed to be incompressible during the irreversible transformation of the porous elementary volume. In the framework of infinitesimal elastic strains, it is possible to assign the following relation, where $J \approx J^{ir}$ was taken into account.

$$\varphi = 1 - \frac{1-\phi_0}{J^{ir}} \tag{9}$$

In the present constitutive model, plasticity is used to model purely mechanical deformation while viscoplasticity represents the chemo-mechanical deformation induced by Intergranular Pressure-Solution. The plastic behavior of the porous material is based on the modified Cam-Clay model (Wood, 1990). The yield surface is given by:

$$f^p\left(\underline{\underline{\sigma}}', p_c\right) = \frac{3}{2}\underline{\underline{s}} : \underline{\underline{s}} + M_{cs}^2 p'\left(p' + p_c\right) \tag{10}$$

where p_c is the consolidation pressure and represents the hardening parameter of the model. The constant M_{cs} is the slope of the critical state line. The plastic criterion depends on the Terzaghi effective stress $\underline{\underline{\sigma}}' = \underline{\underline{\sigma}} + p\underline{\underline{1}}$. The deviatoric stress tensor $\underline{\underline{s}}$ and the mean effective stress p' are given:

$$\underline{\underline{s}} = \underline{\underline{\sigma}} - \frac{1}{3}\mathrm{tr}\underline{\underline{\sigma}}\ \underline{\underline{1}} \qquad\qquad p' = \frac{1}{3}\mathrm{tr}\underline{\underline{\sigma}}' \tag{11}$$

The associated plastic flow rule reads:

$$\underline{\underline{d}}^p = \dot{\chi}\frac{\partial f^p}{\partial \underline{\underline{\sigma}}'}, \text{ with } \dot{\chi} \geq 0 \tag{12}$$

The flow rule for plastic part of porosity change stems from the incompressibility of the solid phase during the irreversible transformation:

$$\dot{\phi}^p = J^p\ \mathrm{tr}\underline{\underline{d}}^p \tag{13}$$

The hardening law is object of special concern. Based on micromechanical reasoning, a specific formulation has been developed for the evolution of p_c by determining the limit load of a hollow sphere subjected to large isotropic compression (Barthélémy et al., 2003). The advantage of this hardening law with respect to classical ones lies in the fact that it avoids the development of negative porosities under high isotropic compression (Deudé et al., 2004). By considering mechanical and chemo-mechanical deformation, the evolution of the hardening parameter is associated with plastic and viscoplastic deformation through J^{ir} as both phenomena contribute to porosity closure. More precisely, the consolidation pressure predicted by (14) tends towards infinity when the pore space vanishes (i.e. $J^{ir} \approx J \to 1-\phi_0$).

$$p_c\left(J^{ir}\right) = \frac{p_{c0}}{\ln\left(\phi_0\right)}\ln\left(1 - \frac{1-\phi_0}{J^{ir}}\right) \tag{14}$$

The viscoplastic component of the strain rate is formulated based on the framework of generalized Perzyna's overstress theory (Perzyna, 1966) with an associated flow rule:

$$\underline{\underline{d}}^{vp} = \frac{1}{\eta_{vp}} \left\langle \Phi(F) \right\rangle^{n} \frac{\partial f_d^{vp}}{\partial \underline{\underline{\sigma}}'} \qquad \dot{\phi}^{vp} = J^{vp} \ \mathrm{tr}\underline{\underline{d}}^{vp} \tag{15}$$

where $\langle\ \rangle$ is the Macaulay brackets, η_{vp} is the viscoplastic viscosity coefficient, n is the viscosity exponent, f_d^{vp} is a dynamic surface defined to describe the current effective stress of the porous material and $\Phi(F)$ is a scaling function that controls the magnitude of viscoplastic strain rate defined as follows (Yin and Hicher, 2008):

$$\Phi(F) = F - 1 = \frac{p_{vp}^{d}}{p_{vp}^{s}} - 1 \tag{16}$$

where p_{vp}^{s} is a static criterion defined to represent the viscoplastic yield surface and p_{vp}^{d} is a dynamic parameter associated to the dynamic viscoplastic surface $f_d^{vp}\left(\underline{\underline{\sigma}}', p_{vp}^{d}\right)$ defined by the modified Cam-Clay model (Adachi and Oka, 1982):

$$f_d^{vp}\left(\underline{\underline{\sigma}}', p_{vp}^{d}\right) = \frac{3}{2}\underline{\underline{s}} : \underline{\underline{s}} + M_{vp}^{2} p'\left(p' + p_{vp}^{d}\right) = 0 \tag{17}$$

where M_{vp} is the slope of the critical state line of the viscoplastic model.

The evolution law for p_{vp}^{s} stems from the heuristic idea that similarity can be preserved between the plastic model used for purely mechanical compaction and the viscoplastic model used for chemo-mechanical compaction. By similarity it is meant that a viscoplastic hardening law having the same structure than (14), which is considered for plastic behavior, can be adopted (Brüch et al., 2016):

$$p_{vp}^{s}\left(J^{ir}\right) = p_{vp0}^{s} \left(\frac{\ln\left(1 - \dfrac{1-\phi_0}{J^{ir}}\right)}{\ln \phi_0} \right)^{m} \tag{18}$$

where scalar m is a material constant, ranging between zero and unity, that controls the relative magnitude of viscoplastic strains (i.e. compaction induced by IPS) with respect to plastic strains (i.e. purely mechanical compaction). Keeping in mind that purely mechanical compaction prevails in the upper layers of the sedimentary basin, the initial value of consolidation pressure p_{vp0}^{s} is physically higher than p_{c0}. From a mathematical viewpoint, viscoplastic strains, that is chemo-mechanical compaction, shall be activated only in layers where condition $p_{vp}^{s}\left(J^{ir}\right) \le p_c\left(J^{ir}\right)$ is satisfied. In particular, this will never occur if $m \ge 1$. In other words, the higher is the value of m, the deeper is the layer of the sedimentary basin for the chemo-mechanical compaction to be activated.

2.1 Porosity effects on the thermo-poro-mechanical properties

Since large irreversible deformations lead to significant changes in porosity, the evolution of the thermo-poro-mechanical properties of the sediment material shall be considered. For sake of simplicity, the anisotropy induced during the loading process is disregarded. Accordingly, the bulk *K* and shear μ moduli of the porous medium appear as functions of the Eulerian porosity φ as well as of the elastic properties of the solid phase k^s and μ^s. More precisely, we adopt herein the Hashin-Shtrikman upper bounds which are known to reasonably model the elastic properties of isotropic porous media (Hashin, 1983):

$$K(\varphi)=\frac{4k^s\mu^s(1-\varphi)}{3k^s\varphi+4\mu^s} \qquad \mu(\varphi)=\frac{\mu^s(1-\varphi)\left(9k^s+8\mu^s\right)}{k^s(9+6\varphi)+\mu^s(8+12\varphi)} \tag{19}$$

Biot coefficient b, Biot modulus M and the thermal dilation coefficient related to the porosity α^ϕ are deduced from the following equations (Coussy, 2004):

$$b(\varphi)=1-\frac{K(\varphi)}{k^s} \qquad M(\varphi)=\frac{k^s}{b(\varphi)-\varphi} \qquad \alpha^\phi(\varphi)=\alpha^s\left(b(\varphi)-\varphi\right) \tag{20}$$

Permeability of saturated porous media is controlled by the interconnected porous space and the viscosity of interstitial fluid η^f. Effects of microstructural changes on the evolution of the permeability coefficient k^f are modeled by means of the Kozeny-Carman formula, where k_0^f is the permeability coefficient at reference porosity ϕ_0 and temperature T_0:

$$\frac{k^f(\varphi,T)}{k_0^f(\phi_0,T_0)}=\frac{\varphi^3(1-\phi_0)^2}{\phi_0^3(1-\varphi)^2}\frac{\eta_0^f(T_0)}{\eta^f(T)} \tag{21}$$

The specific heat of the porous material is defined as a function of the specific heat of the solid and fluid phases, c^s and c^f, weighted by the mass fraction of each constituent as follows (Somerton, 1992):

$$c(\varphi)=\frac{\rho^s(1-\varphi)c^s+\rho^f\varphi c^f}{\rho} \tag{22}$$

The thermal conductivity coefficient k^t is computed based on the micromechanics estimates of Mori-Tanaka which coincide with the upper bounds of Hashin-Shtrikman (Stransky et al., 2011)

$$k^t(\varphi)=k^{t,s}\frac{3k^{t,f}+2(1-\varphi)\left(k^{t,s}-k^{t,f}\right)}{3k^{t,s}+(1-\varphi)\left(k^{t,f}-k^{t,s}\right)} \tag{23}$$

where $k^{t,s}$ and $k^{t,f}$ are the solid and fluid phases thermal conductivity coefficient.

2.2 Temperature effects on the thermo-poro-mechanical properties

Solid phase and skeleton. The evolution of the specific heat of the solid phase is based on the model proposed by Waples and Waples (2004), where c_n^s is a normalized heat capacity:

$$c^s\left(T\right)=c_n^s\left(T\right)\times c^s\left(T=200°\text{C}\right) \tag{24}$$

$$c_n^s\left(T\right)=0.716+1.72\times10^{-3}T-2.13\times10^{-6}T^2+8.95\times10^{-10}T^3 \tag{25}$$

For the thermal conductivity coefficient of the solid phase the following equation is used, where $k_0^{t,s}$ is the thermal conductivity of the solid phase at a reference temperature $T_0\left(°C\right)$ and A is a material constant obtained from laboratory tests (Abdulagatova et al. 2009):

$$k^{t,s}\left(T\right)=\frac{k_0^{t,s}\left(T_0\right)}{1+A\left(T-T_0\right)} \tag{26}$$

The thermal dependency of the viscoplastic viscosity coefficient of the skeleton, which incorporates the different fundamental parameters governing the creep law for IPS is given by an Arrhenius law, where η_{vp0} is the viscosity coefficient at a reference temperature $T_{K,0}\left(K\right)$, with $T_K\left(K\right)=T\left(°C\right)+273.15$ being the temperature in Kelvin, E_a is the activation energy and $R=8.31\ \text{J/K}\times\text{mol}$ is the universal gas constant (Schneider et al., 1996):

$$\eta_{vp}\left(T\right)=\eta_{vp0}\exp\left[\frac{E_a}{R}\left(\frac{1}{T_K}-\frac{1}{T_{K,0}}\right)\right] \tag{27}$$

Fluid phase. In the present work, water is considered to be the only fluid saturating the porous material. It is important to mention that the pore-pressure and temperature state at which the sedimentary basin is subjected in the numerical analysis do not reach the boiling point of water. In addition, water is considered an incompressible fluid with constant density.

The evolution of water specific heat with temperature is obtained from Somerton (1992):

$$c^f\left(T\right)=4245-1.841\ T \tag{28}$$

The thermal conductivity coefficient of water derives from the *International Association for the Properties of Water and Steam* (IAPWS, 1998).

$$k^{t,f}\left(T\right)=0.570+1.616\times10^{-3}T-5.637\times10^{-6}T^2 \tag{29}$$

Viscosity of liquid water in the range of $-24°\text{C}\le T\le373°\text{C}$ is calculated as follows, where $A=141.47\ \mu\text{Pa}\times\text{s}$, $B=226.8\ \text{K}$ and $\alpha=-1.5914$ (Ulamec et al., 2007).

$$\eta^f\left(T\right)=A\left(\frac{T_K}{B}-1\right)^{\alpha} \tag{30}$$

3 FINITE ELEMENT DISCRETIZATION

Assessment of the thermo-poro-mechanical state requires the determination of the temporal evolution of the geometric transformation as well as pore-pressure and temperature changes. This shall be achieved by solving the boundary value problem defined by the set of governing equations together with the constitutive and complementary equations. The particularity of large strains is that all equations actually refer to the mechanical system in its current configuration, which is a priori unknown. The finite element procedure used for assessing the evolution of the porous medium under consideration will be briefly outlined hereafter (Bernaud et al., 2002; Bernaud et al., 2006; Brüch et al., 2016).

The analysis is based on the implementation of the updated Lagrangian scheme (Bathe, 1996). This approach is based on the same procedures used by total Lagrangian formulations, but instead of being referred to the initial configuration, all static and kinematic variables are referred to the last calculated configuration, say at time *t*. The unknown variables are then updated in each time step Δt. The discretized form of the problem is obtained from weak formulation of the momentum, mass and entropy balance equations at time $t+\Delta t$.

Twenty-nodes hexahedra are used for geometry discretization (Fig. 2). A piecewise quadratic polynomial function is adopted to approximate the displacement, while piecewise linear function is adopted for pore-pressure and temperature variations. The resulting systems from finite element discretization are presented in (31) and (32), where $\underline{\underline{K}}_{IJ}$ are the global stiffness sub-matrices and $\underline{F}_I$ the global force sub-vectors. Global vectors $\underline{\mathcal{U}}$, $\underline{\mathcal{P}}$ and $\underline{\mathcal{T}}$ are the nodal displacements, pore-pressure and temperature differences, respectively.

$$\underline{\underline{K}}_{TT} \cdot \underline{\mathcal{T}} = \underline{F}_T \tag{31}$$

$$\begin{bmatrix} \underline{\underline{K}}_{UU} & \underline{\underline{K}}_{UP} \\ \underline{\underline{K}}_{PU} & \underline{\underline{K}}_{PP} \end{bmatrix} \begin{bmatrix} \underline{\mathcal{U}} \\ \underline{\mathcal{P}} \end{bmatrix} = \begin{bmatrix} \underline{F}_U - \underline{\underline{K}}_{UT} \cdot \underline{\mathcal{T}} \\ \underline{F}_P - \underline{\underline{K}}_{PT} \cdot \underline{\mathcal{T}} \end{bmatrix} \tag{32}$$

It is emphasized that, for a given configuration at time *t*, system (32) is highly non-linear due to physical non-linearities (plasticity and viscoplasticity) and geometrical non-linearities (large strains). In particular, vectors $\underline{F}_U$ and $\underline{F}_P$ depend on the poro-mechanical problem unknowns, i.e. $\underline{F}_U = \underline{F}_U\left(\underline{\mathcal{U}}, \underline{\mathcal{P}}\right)$ and $\underline{F}_P = \underline{F}_P\left(\underline{\mathcal{U}}, \underline{\mathcal{P}}\right)$. The iterative algorithm implemented in this work for solving system (32) is based on the Modified Newton-Raphson method.

Simulation of sedimentary basins requires dealing with large space domains (kilometric scale) and large time periods (geological time scale). When applied to the simulation of sedimentary basins, the finite element discretization generally leads to large computational problems involving non-linear and time dependent analyses. For the purpose of memory optimization and computational time reduction, a parallel implementation of the finite element approach based on *OpenMP* standard is used for shared memory multiprocessing interface (Chapman et al., 2008). The Compressed Sparse Row *(CSR)* data structure is adopted to store the components of global stiffness matrix. As regards the iterative solver, the solution of systems (31) and (32) is obtained by using the Preconditioned Conjugated Gradient method *(PCG)* with diagonal preconditioning matrix (Saad, 2003).

The time step δt_{UP} used to solve the poro-mechanical problem (32) is based on the characteristic time of fluid mass diffusion Δt_{ref}^{f} and the characteristic relaxation time Δt_{ref}^{vp}:

$$\Delta t_{ref}^{f} = \frac{h^2}{c_m} \qquad \Delta t_{ref}^{vp} = \frac{\eta_{vp}}{E_{oed}} \tag{33}$$

where h is the finite element thickness, c_m is the liquid diffusivity coefficient and E_{oed} the oedometric elastic modulus. Time step δt_{UP} is obtained by applying a search algorithm which aims to identify the finite element that provides the lowest value between Δt_{ref}^{f} and Δt_{ref}^{vp}.

$$c_m = \frac{k^f M E_{oed}}{E_{oed} + Mb^2} \qquad E_{oed} = K + \frac{4}{3}\mu \tag{34}$$

The time step δt_T used to solve the heat conduction problem (31) is based on the characteristic time of thermal diffusion Δt_{ref}^{t}, where α is the thermal diffusivity coefficient:

$$\Delta t_{ref}^{t} = \frac{h^2}{\alpha} \qquad \alpha = \frac{k^t}{\rho c} \tag{35}$$

For synchronization reasons between the poro-mechanical and thermal numerical procedures, time step δt_T is defined as follows. First, a preliminary time step δt_T^* is computed through a search algorithm similar to that used for δt_{UP}. Then, an integer N is calculated and the time step δt_T is obtained to set up the time discretization of the thermal problem:

$$\delta t_T = \frac{\delta t_{UP}}{N} \qquad N = \text{int}\left(\frac{\delta t_{UP}}{\delta t_T^*}\right) + 1 \tag{36}$$

The thermo-poro-mechanical evolution of the basin is calculated in separate modules as depicted in Fig. 1. The numerical tool proceeds as follows: 1) system (31) is solved from t to t' with N time steps δt_T; 2) information is passed to the poro-mechanical module; 3) system (32) is solved from t to $t' = t + \delta t_{UP}$; 4) information in passed to the thermal module.

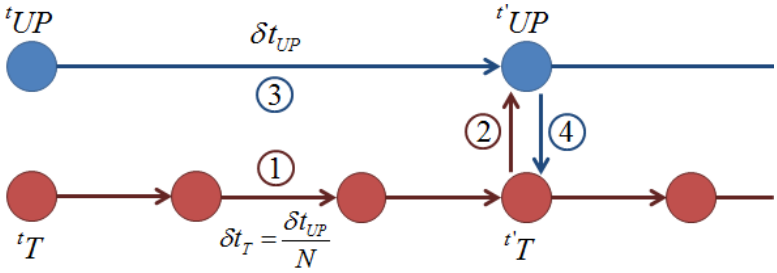

Figure 1. Time discretization scheme for the thermo-poro-mechanical procedure

As the thermo-poro-mechanical properties of the sediment material evolve with porosity and temperature changes, the time steps δt_{UP} and δt_T of the numerical procedure are properly updated during the deformation process and the thermal evolution of the sedimentary basin.

A main specificity of the problem is that sedimentary basins are open systems due to material accretion during the deposition phase. This requires an appropriate technique to overcome the difficulty of dealing with open systems in the context of the finite element method. With the activation/deactivation method used to simulate the accretion process, the real open material system is simulated as a fictitious closed one (Bernaud et al., 2006).

Figure 2 illustrates the basin construction problem, where L_0 indicates the sea level and $H(t)$ corresponds to the top of the sediment layer. The evolution in time of the latter must correspond to that of the real system. The simulation of the accretion phase takes place by subdividing its period T into n subintervals $\left[t_{i-1}, t_i\right]$ with $t_0 = 0$ and $t_n = T$. During the time increment $\Delta t_i = t_i - t_{i-1}$, the sediments supply corresponds to a height of ΔH_i:

$$\Delta H_i = \int_{t_{i-1}}^{t_i} \frac{\dot{M}_d\left(x,y,t\right)}{\rho_0\left(x,y,t\right)} dt \tag{37}$$

where $\dot{M}_d$ is the rate of sediment mass accretion per unit area and ρ_0 represents the mass density of the deposited material.

Before sediment deposition, all finite element layers constituting the system behave as sea water. This is achieved by setting a hydrostatic total stress and pore-pressure state to these elements, in conjunction with sea water density and a high permeability coefficient (compared to the sediment material) $\left|k^f\right| >> k_0^f$. To maintain the proper thermal state and boundary conditions, it is also necessary to set a high conductivity coefficient $\left|k^t\right| >> k_0^t$. For a sea water element (i.e. non-activated element) located at $z = H_i$, stress and pore-pressure are set to:

$$\underline{\underline{\sigma}} = -\rho^f g\left(L_0 - H_i\right)\underline{\underline{1}} \qquad p = \rho^f g\left(L_0 - H_i\right) \tag{38}$$

For every advanced subinterval Δt_i, the thermo-poro-mechanical properties of the deposited material are set to the corresponding layer with thickness ΔH_i. This process starts at the bottom of the basin $\left(z = 0\right)$ and continues upwards until the accretion phase ends.

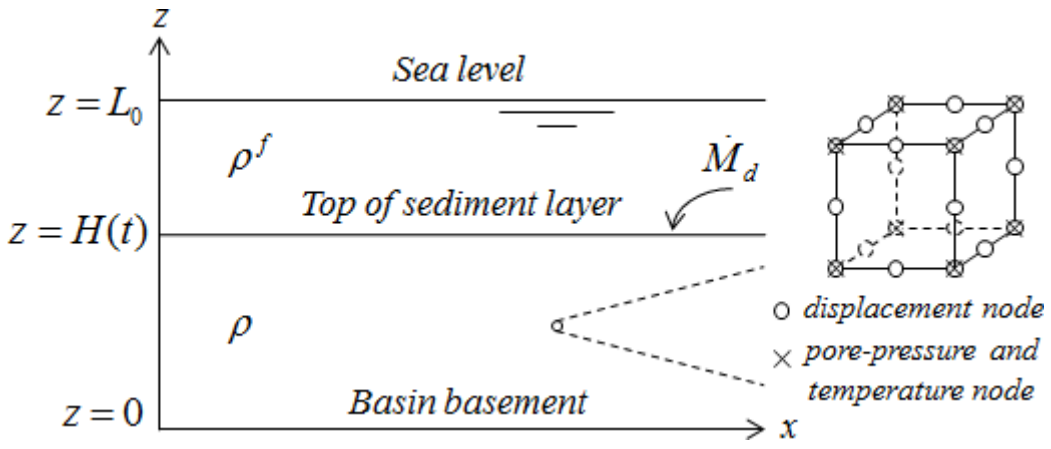

Figure 2. Schematic geometry of the basin and the finite element characteristics

4 COMPUTATIONAL RESULTS

The constitutive model and numerical tool are used to simulate the formation and deformation processes of a sedimentary basin. Lateral-driven deformations generally induced by tectonic sequences are not considered. Since the deformation processes are controlled only by gravitational forces, the analysis is carried out considering oedometric conditions.

The proposed problem lies in a simplified scenario which does not refer to a real basin data. The rate of sediment accretion is constant and equal to $\dot{M}_d = 137$ ton/km^2 per year for a period $t \in [0, T_{sed}]$. The total amount of sediment supply would correspond to a vertical column of thickness $\mathscr{H} = 6000$ m in the absence of compaction, or in other words if the sediment material were rigid. During accretion phase, the sediment material deposited at the top of the basin is assumed to have the same initial properties along geological time scale.

Initial poro-mechanical data are (Brüch et al., 2016): density $\rho_0 = 1.37\times10^3$ kg/m^3, porosity $\phi_0 = 0.72$, Young modulus $E_0 = 10^3$ MPa, Poisson's ratio $\nu_0 = 0.33$, Biot coefficient $b_0 = 0.98$, Biot modulus $M_0 = 2.22\times10^5$ MPa, permeability $k_0^f = 10^{-9}$ MPa^{-1}m^{2}s^{-1}, slope of the critical state line for plasticity $M_{cs} = 1.2$, consolidation pressure $p_{c0} = 1.5$ MPa, slope of the critical state line for viscoplasticity $M_{vp} = 1.2$, static viscoplastic criterion $p^s_{vp0} = 2.0$ MPa, viscoplastic viscosity coefficient $\eta_{vp0} = 1$ GPa$\times$Ma, viscosity exponent $n = 1$, hardening law $m = 0.5$. Sea water density is considered constant $\rho^f = 10^3$ kg/m^3.

The reference temperature for material properties is $T_0 = 0$°C. The specific heat of the solid phase is given by (24) and (25) with $c^s(T = 200\text{°C}) = 1.08\times10^3$ J/kg°C, which provides $c^s_0(T_0) = 7.77\times10^2$ J/kg°C. The thermal conductivity coefficient of the solid phase is obtained from (26) with $k_0^{t,s}(T_0) = 3.44$ W/m°C and $A = 3\times10^{-3}$. At reference temperature, the specific heat and thermal conductivity of water, respectively given by (28) and (29), are $c_0^f(T_0) = 4.24\times10^3$ J/kg°C and $k_0^{t,f}(T_0) = 0.57$ W/m°C. The initial thermal data of the porous material obtained with (22) and (23) are: specific heat capacity $c_0 = 2.6\times10^3$ J/kg°C and thermal conductivity coefficient $k_0^t = 1.2$ W/m°C. Heat generation is disregarded, $r^t = 0$.

Physically speaking, thermal evolution induces unconstrained lateral expansion of the basin. This may be simulated by imposing along the lateral side of geometry model (vertical column) displacements obtained from spatial integration of the heterogeneous strain field $\alpha^s \Delta T \underline{\underline{1}}$. For sake of simplicity, the latter thermal expansion will be neglected in the constitutive state equations: $\alpha^s = 0$ and thus $\alpha^\phi = 0$. Mechanical deformation shall affect the thermal state through geometry and porosity changes. In turn, temperature distribution shall affect the poro-mechanical state of the basin through the temperature dependence law of viscoplastic viscosity coefficient $\eta_{vp}(T)$ (see Eq. (27)) and that of fluid viscosity $\eta^f(T)$ (see Eq. (30)) controlling the permeability of the porous medium (see Eq. (21)). The activation energy considered in Eq. (27) is $E_a = 15\times10^3$ J/mol (Schneider et al., 1996).

The rate of mass accretion $\dot{M}_d$ combined with sediment initial density ρ_0 correspond to an increase of 100 m/My of sediment thickness in unloaded conditions. According to total thickness of deposited material $\mathscr{H}$, the total duration of accretion phase is given by:

$$T_{sed} = \frac{\rho_0 \mathscr{H}}{\dot{M}_d} = 60 \text{ My} \tag{39}$$

The initial geometry of the model consists in a column with 6 km height and horizontal sides $L_x = L_y = 100$ m (actually L_x and L_y values do not matter). The spatial discretization is performed by dividing the column into 60 equal parts in the vertical direction, resulting in cubic hexahedra elements of side $L = 100$ m. The mesh has 728 nodes and 2672 degrees of freedom, of which: 2184 displacements, 244 pore-pressure and 244 temperature unknowns.

The sea bed is located at $z = 0$ and considered rigid and impermeable. The sea level is fixed at $L_0 = 8000$ m. The prescribed temperature at the top of the basin and the upward heat flow applied at the bottom of the basin are assumed constant. In order to represent the basin as a horizontal infinite layer, the geometric model is set under oedometric conditions with impermeable and insulated side surfaces. Figure 3 presents a sketch of the basin geometry in conjunction with the following *a)* poro-mechanical and *b)* thermal boundary conditions:

along $x = 0$ and $x = L_x$: ***a)*** $\underline{\xi} \cdot \underline{e}_x = 0$; $\underline{q}^f \cdot \underline{e}_x = 0$ ***b)*** $\underline{q}^t . \underline{e}_x = 0$ (40)

along $y = 0$ and $y = L_y$: ***a)*** $\underline{\xi} \cdot \underline{e}_y = 0$; $\underline{q}^f \cdot \underline{e}_y = 0$ ***b)*** $\underline{q}^t . \underline{e}_y = 0$ (41)

along $z = 0$: ***a)*** $\underline{\xi} \cdot \underline{e}_z = 0$; $\underline{q}^f \cdot \underline{e}_z = 0$ ***b)*** $\underline{q}^t . \underline{e}_z = 70$ mW/m^2 (42)

along $z = H(t)$: ***a)*** $\underline{T} = -\rho^f g \left(L_0 - H(t)\right) \underline{e}_z$; $p = \rho^f g \left(L_0 - H(t)\right)$ ***b)*** $T = 0°\text{C}$ (43)

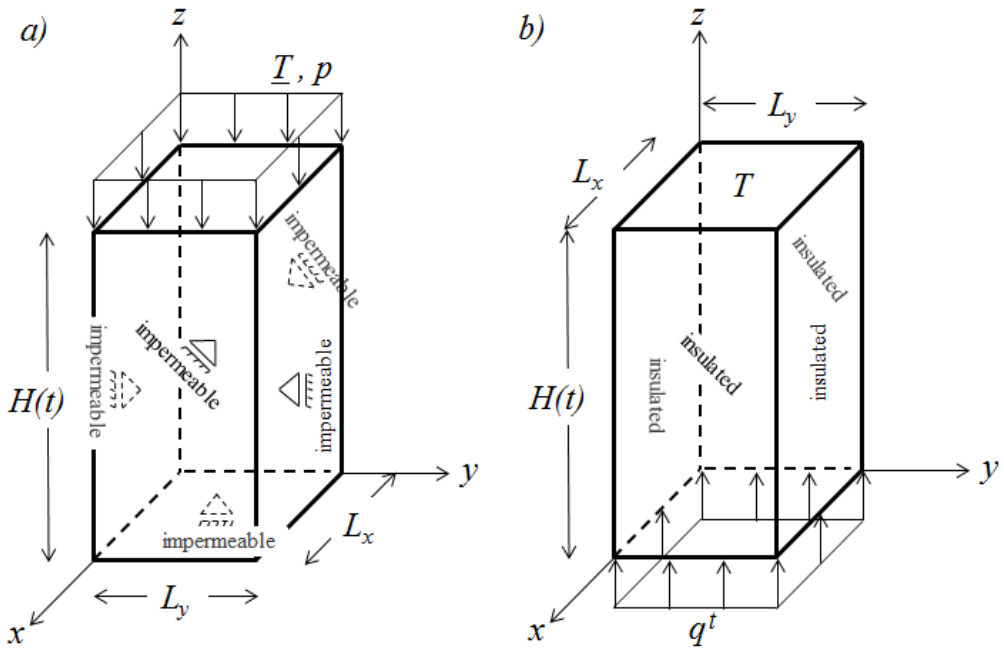

Figure 3. Basin sketch and *a)* poro-mechanical *b)* thermal boundary conditions

To investigate the temperature effects on the deformation processes of the basin, two numerical simulations are presented: a thermo-poro-mechanical analysis in accordance with all data specified so far and a poro-mechanical analysis in isothermal conditions, where the thermal module was kept deactivated in the finite element tool. In what follows, the results associated with the thermo-poro-mechanical analysis are drawn in solid lines, whereas the results concerning the isothermal poro-mechanical analysis are shown in dashed lines.

Figure 4 presents the gravitational compaction law of the basin up to $t = 600$ My. The increasing part of the curve $t \to H(t)$ corresponds to the period $0 \le t \le T_{sed}$ of sediment deposition. The post-peak phase $t > T_{sed}$, during which the sediment supply is interrupted, is characterized by effective stress relaxation induced by IPS and excess pore-pressure dissipation accompanied by continuous compaction of the basin and thus to a significant reduction in its thickness. Once the excess pore-pressure have dissipated and the effective stress relaxation has finished, the hydrostatic regime is recovered after $t = t_\infty$. This last phase corresponds to the horizontal part of the curve and constitutes the long term basin response. We shall refer to this phase as the stabilized or asymptotic basin configuration.

It can be readily observed in Fig. 4 that the incorporation of the temperature effects on the properties of the porous material has significantly accelerated the gravitational compaction processes of the basin. The overall basin deformation may be quantified by the compaction ratio at time t defined as $1 - H(t)/\mathscr{H}$. For the thermo-poro-mechanical analysis, the magnitudes of this ratio at times $t = T_{sed}/2$, $t = T_{sed}$ (end of accretion phase) and $t = 2T_{sed}$ are: 36.6%, 51.6% and 59.3%. For the same times, the overall basin deformation predicted from the isothermal poro-mechanical simulation is: 29.1%, 41.6% and 54.4%. Starting from $\mathscr{H} = 6000$ m of material supply total height, the basin thickness is almost stabilized for both cases at $t = 10T_{sed} = 600$ My, with 60.8% overall deformation for the thermo-poro-mechanical case and 59.8% for the isothermal poro-mechanical case, indicating that the temperature evolution slightly affected the asymptotic configuration of the basin.

The predicted compaction levels are qualitatively compatible with Hamilton's (1959) report which, based on geochemical analysis of several sedimentary basins, has concluded that more than 5 km of clay sediment supply would be necessary to form a basin with stabilized thickness of about 2 km. These compaction ratio levels also emphasize the need to deal with a constitutive model for the sedimentary material formulated in the context of finite strain and taking into account the evolution of the thermo-poro-mechanical properties.

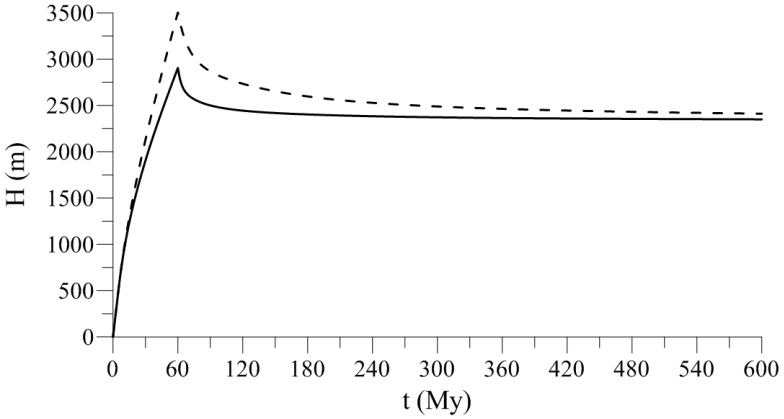

Figure 4. Gravitational compaction law of the basin

Now we focus on analyzing the evolution on time of some fundamental parameters of the porous material constitutive model and the overall behavior of the sedimentary basin which may provide the necessary information to understand the temperature effects on the deformation processes of the basin. The investigation is carried out by presenting some basin profiles at two specific ages, $t = 30$ My and $t = 60$ My, for both numerical simulations.

Figure 5 exhibits the Jacobian of irreversible transformation J^{ir} and Eulerian porosity φ profiles along the basin thickness for the selected ages. Recalling that the porosity law of the constitutive model is function of J^{ir}, it can be observed for both cases and ages that a considerable layer remains in the elastic regime on the upper crust of the basin: while $J^{ir} = J^{p} J^{vp} = 1$ (i.e. plastic and viscoplastic phenomena did not occur) porosity keeps unchanged. This means that the upper layer of the basin remained practically undeformed, as elastic deformation is considered to be infinitesimal in the present model.

The impact of temperature effects on the overall behavior of the basin is noteworthy, as the thermo-poro-mechanical simulation resulted in significantly lower J^{ir} and φ profiles when compared to the isothermal case. The thermal influence on the deformation processes of the basin may be understood as follows: once a layer of sediments is deposited, the heat flow ascending from the deeper layers warms up the porous material, modifying the fluid viscosity and physicochemical properties of minerals. On one hand, the evolution of water viscosity increases the permeability of the deposited layers, which facilitates the dissipation of excess pore-pressure and the load transfer from the pore-fluid to the skeleton of the porous material, increasing the rate of mechanical compaction in the basin. On the other hand, the evolution of the viscoplastic viscosity coefficient leads to higher rates of chemo-mechanical compaction induced by IPS. This can be observed in Fig. 6 which presents the basin profiles of the Jacobian of plastic and viscoplastic deformations, J^{p} and J^{vp}, respectively.

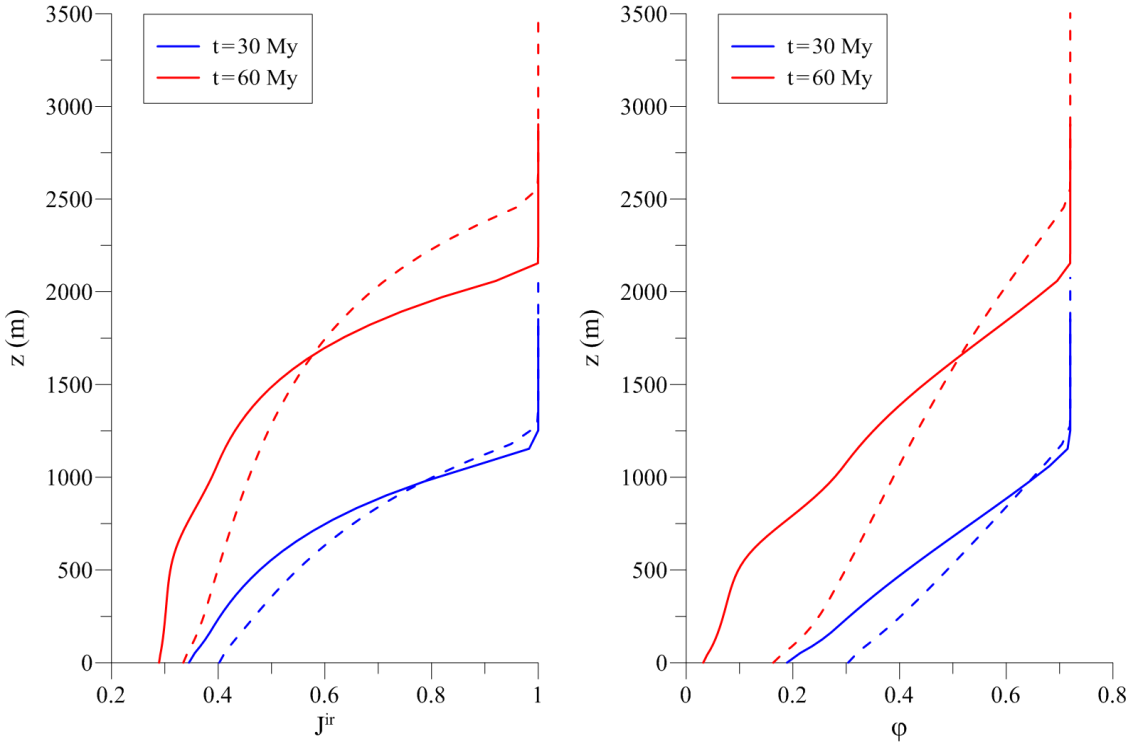

Figure 5. Basin profiles: a) Jacobian of irreversible transformation b) porosity

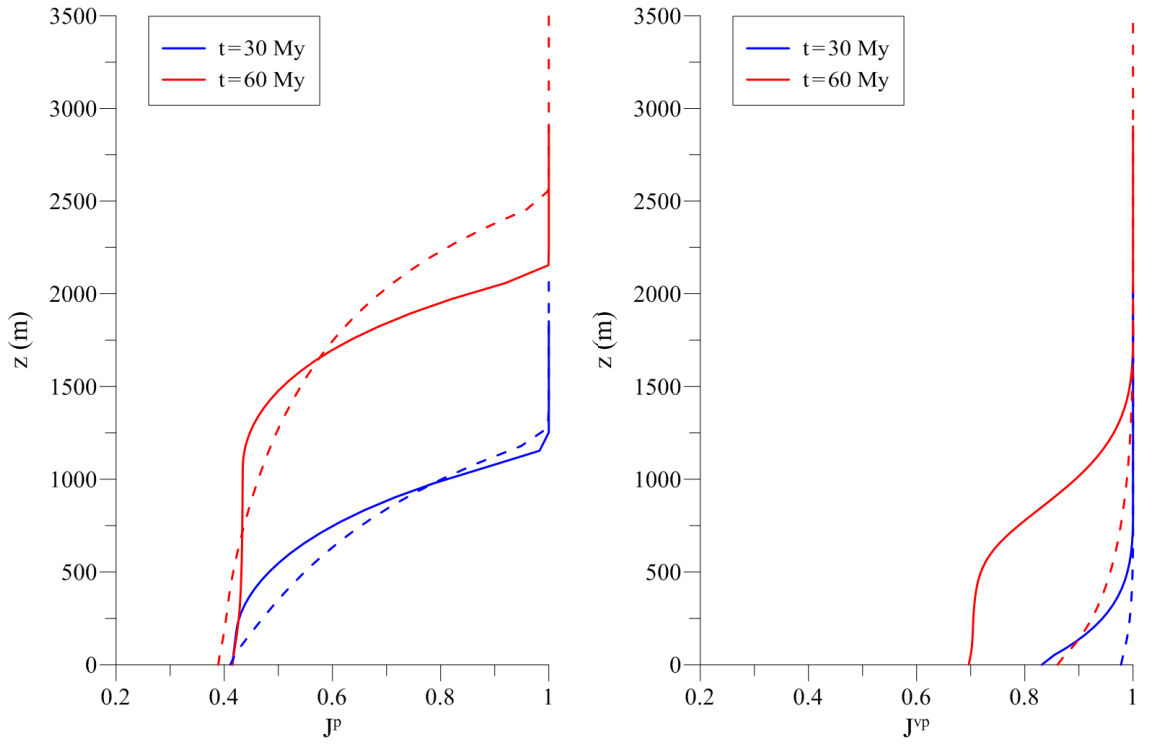

Figure 6. Basin profiles: a) Jacobian of plastic transformation b) Jacobian of viscoplastic transformation

Figure 7 illustrates the profiles of mean effective stress p' along the basin thickness. The p' profiles at $t = 60$ My clearly show the temperature influence on the effective stress relaxation phenomenon, where the isothermal case illustrated in dashed red line presents the smaller values of mean effective stress in the deeper layers of the basin. This is expected as the J^{vp} profile of the thermo-poro-mechanical case presents a noticeable difference in the magnitude of chemo-mechanical deformation in comparison with the isothermal case. This also explains the smaller values of J^{p} presented by the dashed red line at the bottom layer of the basin, where the relaxation phenomenon interrupted the mechanical compaction process earlier in the case which thermal effects are considered. The pore-pressure p profiles presented in Fig. 7 together with the hydrostatic profile demonstrate the excess pore-pressure along the basin thickness which is mainly generated due to sediment supply. One of the consequences of effective stress relaxation associated with Intergranular Pressure-Solution is pore-pressure build-up, as it can be seen at the bottom of the basin for the $t = 60$ My profiles.

The thermal history of the basin is also of great importance as it provides a mean for quantifying the timing of organic maturation, the hydrocarbon generation and also allows evaluation of risk associated with hydrocarbon exploration (Ferrero and Gallagher, 2002). To illustrate the thermal evolution of the basin, Fig. 8 presents the temperature profiles for different selected ages of the thermo-poro-mechanical numerical simulation. It can be observed that, the thicker the basin, the higher is the temperature at the bottom. In addition, the temperature gradients $\partial T/\partial z$ are not constant along the thickness of the basin: although all deposited material has the same initial properties, these properties are modified according to the compaction level of each layer, resulting in a thermal conduction problem of a heterogeneous material. Considering that temperature is prescribed at the top of the basin, $T = 0°\text{C}$, the mean temperature change along the basin thickness at 30, 60, 120 and 600 million years is 46.1, 41.7, 37.7 and 36.7°C/km, respectively.

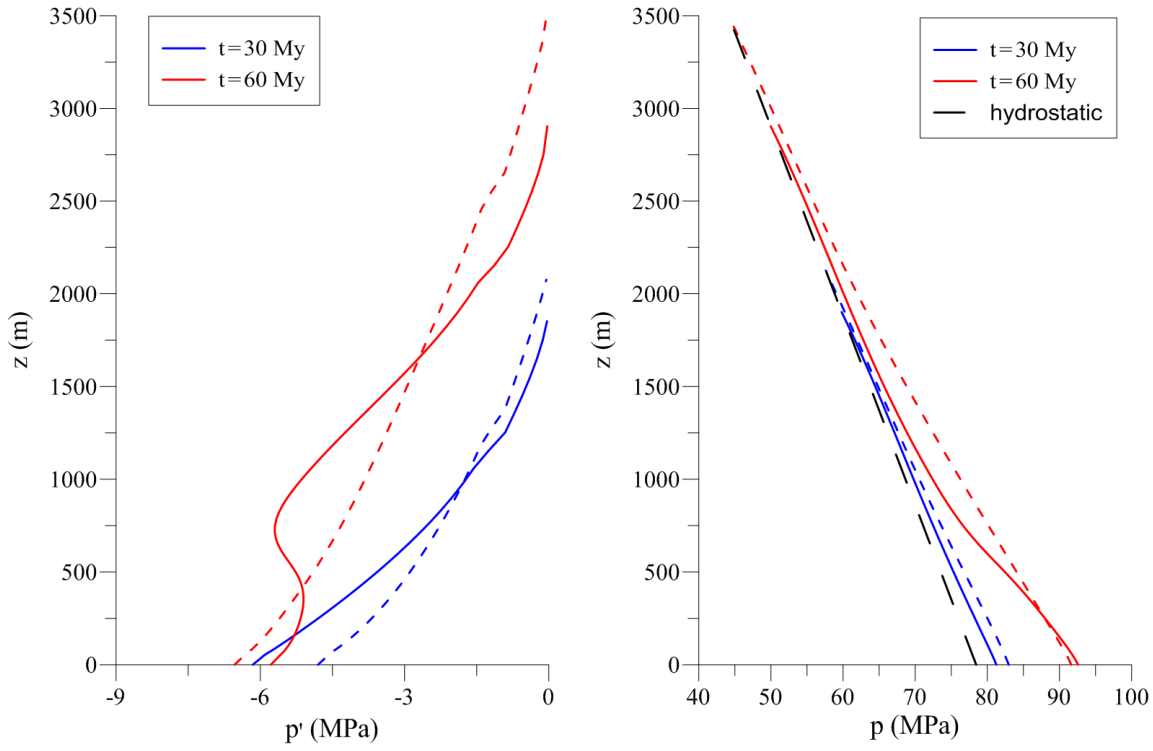

Figure 7. Basin profiles: a) mean effective stress b) pore-pressure

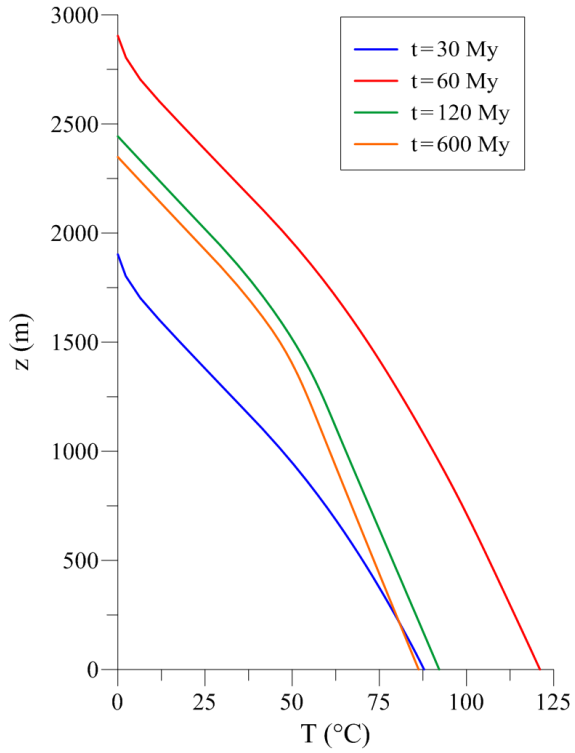

Figure 8. Basin profiles: temperature

5 CONCLUSIONS

The constitutive and computational model presented in Brüch et al. (2016) has been extended to incorporate temperature effects on the porous material behavior to deal with fundamental coupled processes in sedimentary basin modelling such as the compaction of sediments, thermal conduction and fluid flow. Resorting to both micromechanics-based reasoning and phenomenological arguments, the proposed thermo-poro-elasto-visco-plastic constitutive model is formulated within the framework of finite strains and takes into account the evolution of the material properties associated with temperature and porosity changes. The finite element tool has been developed to deal with different processes involved in the life cycle of a sedimentary basin and is potentially able to simulate within a 3D setting the evolution of basins undergoing both gravitational and tectonic-induced deformation.

Temperature effects are incorporated in the constitutive model through partial coupling between the thermal and poro-mechanical evolution of the porous material by adding temperature effects on the state equations of the porous material but disregarding the poro-mechanical effects on the local entropy evolution of the porous medium, which resulted in uncoupled thermal and poro-mechanical systems of equations. However, thermal effects are also considered by modifying the fluid viscosity and physicochemical properties of minerals whereas poro-mechanical evolution leads to systematic modification of geometry and sediment material properties on the thermal conduction problem of the basin.

Incorporation of temperature effects on the properties of the porous material has significantly accelerated the deformation processes of the basin. Heating modified the viscosity of water and increased the permeability of the sediment material, accelerating mechanical deformation associated to excess pore-pressure dissipation and rearrangement of solid particles. It has also increased the rates of chemo-mechanical compaction due to thermal dependency of the viscoplastic viscosity coefficient of the skeleton, which incorporates the different fundamental parameters governing the creep law for Intergranular Pressure-Solution.

It should be noted that, although the numerical analysis presented herein refers to a simplified geological scenario regarding the sedimentary basin history, the main features of basin deformation predicted by the finite element simulations are in qualitative agreement with available numerical results and data from real sedimentary basin life: the overall compaction level of the basin and the porosity, pore-pressure, temperature and geothermal gradient profiles. However, the effective validation of the constitutive and computational model remains to be made through comparisons with data from real sedimentary basins.

Some issues remain to be addressed on both theoretical and computational viewpoints. For instance, the implementation of a finite element formulation with enriched interpolation functions like the extended finite element method *(XFEM)* would be suitable to handle the issue of fractures and faults induced by tectonic loading in sedimentary basins.

REFERENCES

Abdulagatova, Z., Abdulagatov, I.M., Emirov, V.N., 2009. Effect of temperature and pressure on the thermal conductivity of sandtone. *International Journal of Rock Mechanics & Mining Sciences*, vol. 46, pp. 1055−1071.

Adachi, T.; Oka, F., 1982. Constitutive equations for normally consolidated clay based on elasto-viscoplasticity. *Soils and Foundations*, vol. 22, n. 4, pp. 57−70.

Barthélémy, J. F.; Dormieux, L.; Maghous, S., 2003. Micromechanical approach to the modelling of compaction at large strains. *Computers and Geotechnics*, vol. 30, pp. 321-338.

Bathe, K.J., 1996. *Finite element procedures*. Prentice-Hall.

Bernaud, D., Deudé, V., Dormieux, L., Maghous, S., Schmitt, D.P., 2002. Evolution of elastic properties in finite poroplasticity and finite element analysis. *International Journal for Numerical and Analytical Methods in Geomechanics*, vol. 26, pp. 845–871.

Bernaud, D., Dormieux, L., Maghous, S., 2006. A constitutive and numerical model for mechanical compaction in sedimentary basins. *Computers and Geotechnics*, vol. 33, pp. 316–329.

Bjorlykke, K., 2010. *Petroleum geoscience: from sedimentary environments to rock physics*. Springer: Berlin.

Brüch, A., Maghous, S., Ribeiro, F.L.B., Dormieux, L., 2016. A constitutive model for mechanical and chemo-mechanical compaction in sedimentary basins and finite element analysis. *International Journal for Numerical and Analytical Methods in Geomechanics*, DOI: 10.1002/nag.2530.

Chapman, B., Jost, G., Pas, R. van der, 2008. *Using OpenMP: portable shared memory parallel programming*. The MIT Press: Cambridge.

Coussy, O., 2004. *Poromechanics*. John Wiley & Sons Ltd: Chichester.

Deudé, V.; Dormieux, L.; Maghous, S.; Barthélémy, J. F.; Bernaud, D., 2004. Compaction process in sedimentary basins: the role of stiffness increase and hardening induced by large plastic strains. International *Journal for Numerical and Analytical Methods in Geomechanics*, vol. 28, pp. 1279-1303.

Dormieux, L., Maghous, S., 2000. Evolution of elastic properties in finite poroplasticity. *C.R. Acad. Sci. Paris*, vol. 328, n. IIb, pp. 593–600.

Ferrero, C., Gallagher, K., 2002. Stochastic thermal history modelling. 1. Constraining heat flow histories and their uncertainty. *Marine and Petroleum Geology*, vol. 19, pp. 633–648.

Hamilton, E.L., 1959. Thickness and consolidation of deep-sea sediments. *Bulletin of the Geological Society of America*, vol. 70, pp. 1399–1424.

Hashin, Z., 1983. Analysis of composite materials - a survey. *Journal of Applied Mechanics*, vol. 50, pp. 481-505.

IAPWS, 1998. Revised release on the IAPS formulation 1985 for the thermal conductivity of ordinary water substance. *Releases of the International Association for the Properties of Water and Steam*.

Palumbo, F., Main, I.G., Zito, G., 1999. The thermal evolution of sedimentary basins and its effect on the maturation of hydrocarbons. *Geophysical Journal International*, vol. 139, pp. 248–260.

Perzyna, P., 1966. Fundamental problems in viscoplasticity. *Advances in Applied Mechanics*, vol. 9, pp. 243–277.

Saad, Y., 2003. *Iterative Methods for Sparse Linear Systems*. 2nd ed. Society for Industrial and Applied Mathematics: Philadelphia.

Schmidt, V., McDonald, D.A., 1979. The role of secondary porosity in the course of sandstone diagenesis. *Aspects of Diagenesis*, vol. 26, pp. 175–207.

Schneider, F., Potdevin, J.L., Wolf, S., Faille, I., 1996. Mechanical and chemical compaction model for sedimentary basin simulators. *Tectonophysics*, vol. 263, pp. 307–317.

Somerton, W.H., 1992. *Developments in petroleum science V.37: thermal properties and temperature-related behavior of rock/fluid systems*. Elsevier: Amsterdam.

Stransky, J., Vorel, J., Zeman, J., Sejnoha, M., 2011. Mori-Tanaka based estimates of effective thermal conductivity of various engineering materials. *Micromachines*, vol. 2, n. 2, pp. 129–149.

Ulamec, S., Biele, J., Funke, O., Engelhardt, M., 2007. Access to glacial and subglacial environments in the Solar System by melting probe technology. *Reviews in Environmental Science and Bio/Technology*, vol. 6, pp. 71–94.

Waples, D.W., Waples, J.S., 2004. A review and evaluation of specific heat capacities of rocks, minerals, and subsurface fluids. Part 1: minerals and nonporous rocks. *Natural Resources Research*, vol. 13, n. 2, pp. 97–122.

Wood, D.M., 1990. *Soil Behaviour and critical state soil mechanics*. Cambridge University Press: Cambridge.

Yin, Z.Y., Hicher, P.Y., 2008. Identifying parameters controlling soil delayed behaviour from laboratory and in situ pressuremeter testing. *International Journal for Numerical and Analytical Methods in Geomechanics*, vol. 32, pp. 1515–1535.